

FIBRILLATION OF FLAX AND WHEAT STRAW CELLULOSE: EFFECTS ON THERMAL, MORPHOLOGICAL, AND VISCOELASTIC PROPERTIES OF POLY(VINYLALCOHOL)/FIBRE COMPOSITES

Marta Hrabalova,^{a,*} Manfred Schwanninger,^b Rupert Wimmer,^{a, c} Adriana Gregorova,^d Tanja Zimmermann,^e and Norbert Mundigler^a

Nano-fibrillated cellulose was produced from flax and wheat straw cellulose pulps by high pressure disintegration. The reinforcing potential of both disintegrated nano-celluloses in a polyvinyl-alcohol matrix was evaluated. Disintegration of wheat straw was significantly more time and energy consuming. Disintegration did not lead to distinct changes in the degree of polymerization; however, the fibre diameter reduction was more than a hundredfold, creating a nano-fibrillated cellulose network, as shown through field-emission-scanning electron microscopy. Composite films were prepared from polyvinyl alcohol and filled with nano-fibrillated celluloses up to 40% mass fractions. Nano-fibrillated flax showed better dispersion in the polyvinyl alcohol matrix, compared to nano-fibrillated wheat straw. Dynamic mechanical analysis of composites revealed that the glass transition and rubbery region increased more strongly with included flax nano-fibrils. Intermolecular interactions between cellulose fibrils and polyvinyl alcohol matrix were shown through differential scanning calorimetry and attenuated total reflection-Fourier transform infrared spectroscopy. The selection of appropriate raw cellulose material for high pressure disintegration was an indispensable factor for the processing of nano-fibrillated cellulose, which is essential for the functional optimization of products.

Keywords: Polyvinyl alcohol; Nano-fibrillated cellulose; Composite film; Viscoelastic properties; Thermal properties; Film; ATR-FTIR

Contact information: a: Institute for Natural Materials Technology, IFA-Tulln, University of Natural Resources and Life Sciences, Vienna, Konrad Lorenz Strasse 20, A-3430 Tulln, Austria; b: Department of Chemistry, BOKU – University of Natural Resources and Life Sciences, Vienna, Muthgasse 18, A-1190 Vienna, Austria; c: Faculty of Forest Sciences and Forest Ecology, University of Göttingen, Büsgenweg 4, 37077 Göttingen, Germany; d: Institute for Chemistry and Technology of Materials, Graz University of Technology, Stremayrgasse 9, 8010 Graz, Austria; e: Empa, Swiss Federal Laboratories for Materials Science and Technology, Wood Laboratory, Ueberlandstrasse 129, CH-8600 Dübendorf, Switzerland; *Corresponding author: martahrabalova@hotmail.com

INTRODUCTION

Cellulose is the most abundant naturally occurring polymer on earth. The average plant contains roughly 40% of cellulose, which adds up to bio-based resource of approximately 2000 million dry tons (Rowell et al. 2000). During the past years a lot of research on the disintegration of cellulose fibres through chemical (Samir et al. 2005) or mechanical treatments such as high pressure disintegration (Siró and Plackett 2010) has

been performed. Due to the absence of imperfections that originated from chain folding, the obtained fibres should demonstrate unique properties similar to the perfect crystal of native cellulose (Nakagaito & Yano 2005). Chemical treatments have led to uniformly sized cellulose whiskers of lower aspect ratios (Favier et al. 1995; Helbert et al. 1996), while mechanical refining or homogenization processes results in nano-fibrillated cellulose (NFC) fibrils with a wide size distribution and also higher aspect ratio (Nakagaito and Yano 2004). Today, high pressure fibrillation is the most common method for producing nano-sized cellulose materials with applications in food industry, cosmetics or pharmaceutical industry (Nakagaito and Yano 2005). Structural features of cellulosic fibres and the ability to form a variety of intermolecular interactions with other materials are fundamental aspects for good adhesion between fibre and matrix, which greatly improve performance of fibre reinforced composites (Iwamoto et al. 2007; Lu et al. 2008; Schartel et al. 1996).

With the use of hydrophilic-type matrices such as polyvinyl alcohol (PVA) higher compatibility as well as better fibre dispersion is possible. In addition, the obtained composite material is environmentally friendly and processable at ambient conditions (Yu et al. 2006). Due to their hydrophobicity PVA/nano-cellulose composites are suitable for the production of medical device applications.

PVA is a water-soluble and highly biodegradable polymer prepared through hydrolysis of polyvinyl acetate. PVA has excellent antistatic and oxygen barrier properties and it is resistant to most organic solvents (Moore et al. 1997). Due to its hydrophilicity PVA is also suitable for the production of nano-composites that are destined for biomedical applications (Millon & Wan 2006; Galya, et al. 2008). NFCs made from different raw materials have been utilized with PVA as a matrix, including commercially microfibrillated cellulose (Lu et al. 2008), nano-fibrillated wood (Zimmermann et al. 2004), nano-fibrillated sugar beet pulp (Leitner et al. 2007) or fibrils from Swede roots (Bruce et al. 2005) NFCs. It was shown that the choice of fibre raw material affects processing parameters, including energy consumption, the latter being critical when used industrially (Zimmermann et al. 2010). The objectives of this work are (1) to apply the fibrillation process to two types of cellulose fibres, (2) to produce nano-composites with the two reinforcing fibre types in PVA matrices, (3) to determine thermal, morphological and viscoelastic properties of obtained composite materials, and (4) to determine water uptake sensitivity at a given climate change.

It is known that different types of cellulose may show a diversity of functions in composites (Klemm et al. 2009). Therefore, cellulose pulps from flax (F) and wheat (WS) were used as raw materials. The two nano-fibrillated fibre types were incorporated into PVA matrices at NFC mass fractions (w_C) ranging between 5 and 40%. The impact of a wide range of NFC content on properties of PVA/NFC composites was assessed. Reinforcing potential of NFCs for hydrophilic PVA matrix was particularly determined by dynamic mechanical analysis (DMA). Further thermal properties of PVA/NFC were observed using differential scanning calorimetry (DSC). Cellulose dispersion in the PVA matrix was studied through scanning electron microscopy (NanoSEM); and intermolecular H-bondings were identified through Attenuated Total Reflection-Fourier Transform InfraRed Spectroscopy (ATR-FTIR). Cellulose polymerization degree (DP) was determined by viscosimetry, and structural order was assessed by ATR-FTIR.

Cellulose structures were identified through field emission scanning electron microscopy (FE-SEM).

EXPERIMENTAL

Materials

Poly(vinyl alcohol) Airvol 523 (medium viscosity, degree of hydrolysis 86% to 88% and average molecular weight ~ 89,000) was supplied by AIR Products and Chemicals, Inc. (USA). For the isolation of nanofibrillated cellulose two commercially available pulps obtained from wheat straw (*Tritium vulgare*) and flax (*Linum usitatissimum*) were provided by the Delfort group AG (Austria).

Methods

High pressure disintegration of cellulose fibres

Both pulp types were swollen in deionised water in a 10 L thermostatic reactor and stirred. To obtain a more homogeneous suspension, a big-sized Ultra-Turrax (T 50 BASIC IKA WERKE) was used. The suspension was then passed through an inline dispersion system, equipped with the Ultra-Turrax Megatron MT 3000 (Kinematica AG, Switzerland), which was attached to a thermostatic reactor. Inline dispersion was performed between 15,000 rpm and 20,000 rpm to disintegrate the fibres. The temperature of the system was kept at 15 °C to avoid growth of bioactive organisms. Finally, the fibre suspension was passed through a high-pressure homogenizer (Microfluidizer, M-110Y). The exact apparatus configuration is described elsewhere (Zimmermann et al. 2010). The resulting suspensions were centrifuged several times at 5,000 rpm for 20 minutes at temperature of 20 °C, until 5.95% dry matter content was reached for the nanofibrillated wheat straw pulp (WS-NFC) and 9.75% for nanofibrillated flax pulp (F-NFC).

Viscosimetric measurements

The intrinsic viscosity of both non-fibrillated and fibrillated celluloses was determined according to ISO 5351 standard (Anonymous 2004). Degree of polymerization (DP) was then calculated using the Staudinger-Mark-Houwink equation,

$$[\eta] = (K * DP)^a \quad (1)$$

where the constants K and a depend on the polymer-solvent system (Henriksson 2008). For wheat straw $K = 2.28$ and $a = 0.76$, while for flax $K = 0.42$ and $a = 1$, respectively (Marx-Figini 1978).

Field emission scanning electron microscopy (FE-SEM)

Aqueous cellulose suspensions of 0.1% cellulose mass fraction were dropped on a specimen holder and directly sputtered with a 7.5 nm thick platinum layer (BAL-TEC MED 020 modular high vacuum coating systems, BALTEC AG, Principality of Liechtenstein). Microscopic analysis was accomplished for all cellulose materials prior

and post disintegration using a Jeol 6300F (Jeol Ltd., Japan), operated under high vacuum at 5kV beam voltage. Diameter of the fibres was determined from SEM images with 20,000 and 10,000 magnifications, respectively. Images were analysed using Adobe Acrobat 7.0 Professional software, and averages were built from measurement of 200 fibres.

Composite preparation

A 3.3%-PVA solution was prepared by stirring PVA in deionised water at room temperature for 6 hours. The suspension with $w_C = 0.5\%$ of NFC was prepared with deionized water by stirring the cellulose for 6 hours. The suspension was treated by a touch mixer (VORTEX-GENIE 1 Touch Mixer) for 5 minutes and dispersed with the Ultra-Turrax IKA T10 basic for 2 minutes to achieve high homogeneity. PVA solution was mixed with appropriate amounts of NFC aqueous suspension to prepare composite films with a final NFC contents ranging between 0 and 40%. The PVA/NFC suspensions were stirred for 16 hours, then cast in Teflon forms and finally dried at 50% relative humidity (RH) and 23°C up to 7 days. In addition to PVA/NFC films neat cellulose films were also cast from a $w_C = 0.5\%$ non-fibrillated cellulose suspension, as well as from a 0.5% NFC suspension. After water evaporation, all films were dried under vacuum for 24 hours at 40 °C. Prior to testing, the obtained composite sheets were kept in a desiccator with dried silica gel to avoid water swelling and consequently plastification of the PVA matrix. The different sample groups were marked as follows: F-NFC for neat nano-fibrillated flax cellulose films, WS-NFC for neat nano-fibrillated wheat straw cellulose films, and PVA for neat polyvinyl alcohol film. PVA/xF-NFC, PVA/xWS-NFC stand for PVA composite films with nano-fibrillated flax and wheat straw cellulose, respectively, having a x-percent mass fraction of NFC in the composite.

ATR-FTIR spectroscopy

The ATR-FTIR spectra of films were measured with 32 scans per sample at a spectral resolution of 4 cm^{-1} and a wavenumber range between 4000 cm^{-1} to 600 cm^{-1} . An attenuated total reflectance (ATR) device (MIRacle™, from Pike Technologies, www.piketech.com) was installed on a Bruker Vertex 70 device (Bruker Optics, www.brukeroptics.de), together with a DLATGS mid-infrared detector. Four spectra were recorded for each film and averaged. For the calculation of relative crystallinity the spectra obtained from cellulose films were minimum-maximum normalized over the whole wavenumber range. Baseline correction was performed by the rubber-band method to minimize differences between spectra due to baseline shifts (Erukhimovitch et al. 2006). Composition dependent spectra of O-H stretching region were minimum-maximum corrected in the wavenumber range between 3800 cm^{-1} and 3000 cm^{-1} .

Scanning electron microscopy (NanoSEM)

Composite films were cryo-fractured in liquid nitrogen and fracture surfaces were sputtered with 7.5 nm platinum layer. Fractured surfaces of the PVA/NFC composites were studied with a reflection electron microscope, FEI Nova NanoSEM 230.

Water-uptake

Relative water uptake measurements were performed on films sized 20 mm x 20 mm and a thickness of about 0.20 mm. Dry weight of each sample was over 100 mg. After dry weighing, the samples were placed in a conditioned room with 50% relative humidity and 23°C. Weight changes of the nano-fibrillated celluloses, PVA and the PVA/NFC composites samples were measured up to 9 days with the moisture content determined as follows,

$$wt.\% = 100 * \frac{W_2 - W_1}{W_1} \quad (2)$$

where W_1 is the weight of the dry sample, and W_2 the weight of the wet sample.

Differential scanning calorimetry (DSC)

Melting behaviour of the PVA and PVA/NFC composite films was studied on a NETZSCH DSC 200 F3 Maja. Approximately 8 mg of sample was sealed in pierced aluminium pans. Measurements were conducted within the temperature range of 20 °C and 220 °C at a heating rate of 10 K/min, and a nitrogen gas flow of 20 mL/min. Melting temperature (T_m) was derived from the melting peak. Heat of fusion (ΔH_m) was evaluated from the peak area with respect to the PVA mass fraction in the composite film. Results are reported as average values of duplicate measurements. The maximal experimental error of T_m data was indicated to be $\pm 0.5^\circ\text{C}$ and $\pm 1 \text{ J/g}$ of ΔH_m .

Dynamic-mechanical analysis (DMA)

Viscoelastic properties of PVA/NFC composite films were measured on a NETZSCH 242 C in tensile mode. Strips of 10 mm \times 6 mm \times 0.1 mm in size were cut. Storage modulus (E'), and the height of loss tangent peak ($\tan \delta$) were measured within the temperature range of -20 °C to 120 °C at a strain sweep frequency of 1 Hz and a heating rate of 3 °C/min. Glass transition temperature (T_g) was evaluated from the E' inflection point.

RESULTS AND DISCUSSION

Processibility of nano-fibrillated cellulose

Flax cellulose was chosen because of its excellent mechanical properties and outstanding reinforcement potential (Charlet et al. 2010), while wheat straw cellulose as residual agricultural material seemed to be an economically and environmentally viable source of cellulose (Liu et al. 2005). Processing conditions for each material are listed in Tables 1 and 2.

Cellulose pre-processing involved the swelling followed by several disintegration steps. Pre-processing procedures were necessary to obtain homogeneous cellulose suspensions, making it possible to pass through the high pressure homogenizer. As water penetrated the amorphous cellulose regions, hydrogen bonds were disrupted and distances between cellulose chains loosened (Timár-Balázs and Eastop 2002), which

eased mechanical disintegration. The compliancy of the wheat straw slurry to pass the inline disperser turned out to be low; therefore, the time of WS swelling was 4 times longer than for flax. In addition, due to repeated chamber clogging when passing WS through the high pressure homogenizer, the required time for inline dispersion of the WS slurry was also markedly longer than for the F slurry. To lower the chance of chamber clogging the WS slurry was diluted to a mass fraction of 0.375%.

Table 1. Processing Conditions upon Mechanical Pre-treatment

Material	Swelling		Ultra-Turrax (big)		Inline dispersion	
	Cellulose mass fraction in slurry [%]	Time [h]	Cellulose mass fraction in slurry [%]	Processing time [h]	Cellulose mass fraction in slurry [%]	Processing time [h]
F	1	62	1	5	1	6.5
WS	0.8	254	0.8	6	0.8	9.2

Table 2. Chamber Combinations Used during High Pressure Disintegration.

Chamber combinations	F slurry (No. of passes)	WS slurry (No. of passes)
400 μm + 200 μm	12	14
400 μm + 75 μm	0	8
200 μm + 75 μm	12	0

The mass fraction of F and WS in slurry during processing was 1% and 0.375%, respectively.

During the final high pressure disintegration step (using the interaction chamber combinations 200 μm + 75 μm for F, and 400 μm + 75 μm for WS), 100 g of flax dry matter has passed through within 18 minutes, whereas the same amount of WS took 70 minutes. For both celluloses the high pressure fibrillation was interrupted on the basis of visual evaluation as soon the suspension was homogeneous and free of agglomerates. The absence of agglomerates was continuously checked by rubbing the suspension between two fingers (Zimmermann et al. 2010).

Table 3. Intrinsic Viscosity $[\eta]$ and DP of Wheat Straw and Flax Celluloses

Material	$[\eta]$ [mL/g]	DP
F	300	714
F-NFC	290	691
WS	710	1,909
WS-NFC	640	1,665

Degree of polymerization (DP)

Through viscosimetric measurements the DPs for both raw materials were obtained. Overall, the DP of flax cellulose was markedly lower than that of wheat straw cellulose (Table 3). As DP predicates, the stiffness of cellulose chain having higher DP for WS cellulose might explain the difficulties present during processing. Changes of DP induced by fibrillation were rather small for both materials (3.2% for F and 12.8% for WS) and indicate breakage along the fibre (Iwamoto et al. 2007). The DP drop due to high pressure disintegration was more pronounced for higher DP material, which was in accordance with the findings of Zimmermann et al. (2010).

Morphology of the fibres

The structural nature of the non-fibrillated F and WS celluloses and effects of high pressure treatment on their structure are shown in Fig. 1. Fibre diameter prior to fibrillation was around 12 μm for F cellulose, and 18 μm for WS cellulose. After high pressure disintegration the obtained fibrils had diameters markedly different from the previous fibres. For F-NFC the fibril diameters ranged between 37 nm and 430 nm (average 81 nm), and for WS-NFC between 60 nm and 1,080 nm (average 128 nm). Fraction of fibrils reaching nanometer dimension (<100nm) was determined to be 82% for F-NFC, and to be 58% for WS-NFC, respectively. The increased variability was due to the fact that the fibrils remained partly as agglomerates. Even with the presence of agglomerated fibrils the homogenization process greatly increased the surface area.

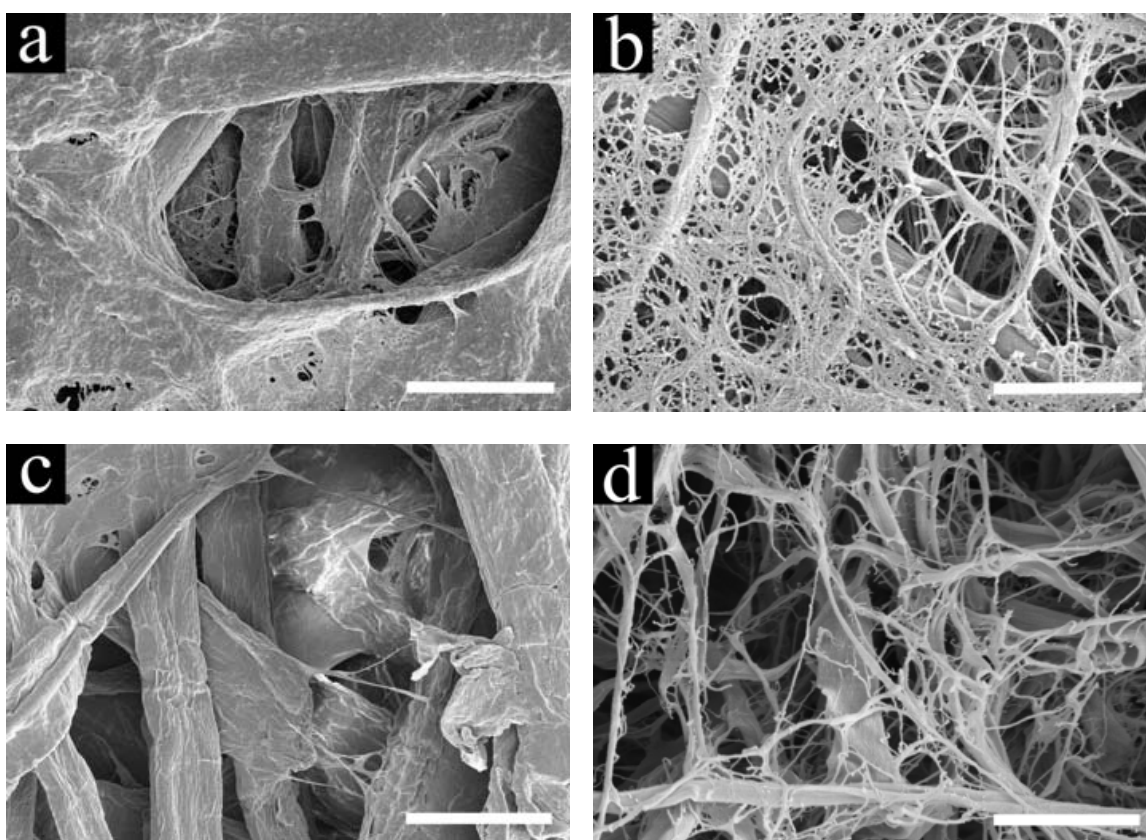


Fig. 1. FE-SEM micrographs of a) F cellulose non-fibrillated, b) F-NFC, c) WS cellulose non-fibrillated, d) WS-NFC. The white scale bar represents the length of 20 μm (a and c) and 3 μm (b and d)

Table 4. Changes of Relative Crystallinity due to Fibrillation Determined by ATR-FTIR

Cellulose	$A_{1400-1289}/A_{898}$
F	5.8
F-NFC	5.4
WS	4.0
WS-NFC	3.8

ATR-FTIR analysis of celluloses and composites

Normalized spectra of NFC and non-fibrillated cellulose sheets acquired for the wavenumber range 1800 cm^{-1} to 600 cm^{-1} are shown in Fig. 2. Spectral profiles in this region turned out to be very similar; however, band intensities were slightly changed. Relative crystallinity of both materials before and after high pressure disintegration was calculated from band area ratios $A_{1400-1289}/A_{898}$ (Schwanninger et al. 2004). Schultz et al. (1985) report that this ratio correlates well with the crystallinity determined by X-ray diffraction. As can be seen in Table 4, relative crystallinity was found to be higher for the flax cellulose films. Crystallinity decreased after high pressure disintegration for both materials. Similar findings were reported by Iwamoto *et al.* (2007) who measured decline of cellulose crystallinity through X-ray diffraction as a response of high pressure disintegration. Schwanninger *et al.* (2004) reported a decrease in cellulose relative crystallinity due to the ball milling measured by FTIR, which is another confirmation for their own findings.

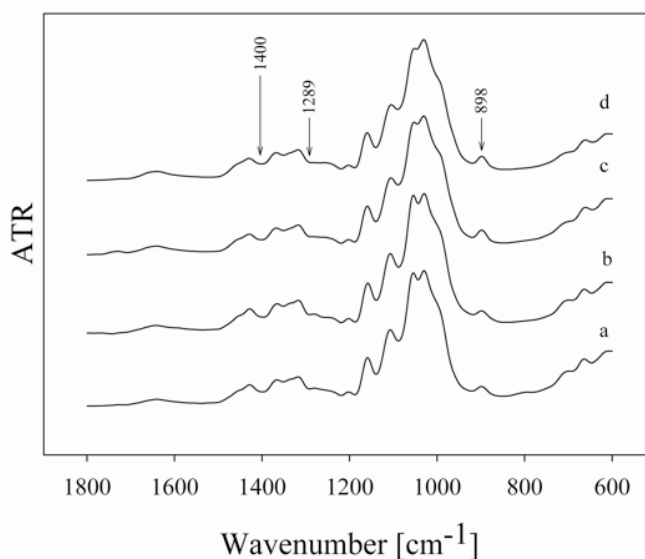


Fig. 2. ATR-FTIR spectra in the range from 1800 cm^{-1} to 600 cm^{-1} of NFC and non-fibrillated cellulose films. a) F-NFC, b) F cellulose non-fibrillated, c) WS-NFC and d) WS cellulose non-fibrillated. (Absorbance scale is not given because spectra are shifted parallel.)

FT-IR is a suitable method for the determination of molecular interactions among various chemical groups and consequently the composite compounds (Kondo et al. 1994; Sawatari and Kondo 1999; Shibayama et al. 1991; Zhu et al. 2003). In PVA/cellulose systems mutual interactions via hydrogen bonding of hydroxyl groups have been reported (Kondo et al. 1994; Shibayama et al. 1991). Using FTIR hydrogen bonding between OH groups can be observed within the O-H stretching range of 4000 cm^{-1} to 3000 cm^{-1} . Normalized FTIR spectra of the O-H stretching region for NFC, PVA, and PVA/NFC with up to $w_C = 40\%$ are shown in Fig. 3, for both nano-composite types. The maximum of cellulose O-H stretching band was situated at 3336 cm^{-1} (at 3342 cm^{-1} O(3)-H(3)···O(5) intra-chain H-bond (Maréchal and Chanzy 2000)), which is close to the hydroxyl stretching vibration of PVA (3325 cm^{-1}) (Tadoroko 1959). The shift of the O-H stretching

peak to the lower wavenumber of 3315 cm^{-1} was observed for PVA/NFC systems containing 5% of cellulose. This shift was accompanied by a broadening of the O-H stretching band in the case of the WS composite. The extended width of O-H stretching band refers to a broader distribution of hydrogen bond lengths, and the shift to a lower wavenumber was due to bond strengthening and shortening. The shift of O-H stretching bands of the composite to a lower wavenumber relative the NFCs and PVA peaks was expected for the composite having a low NFC mass fraction.

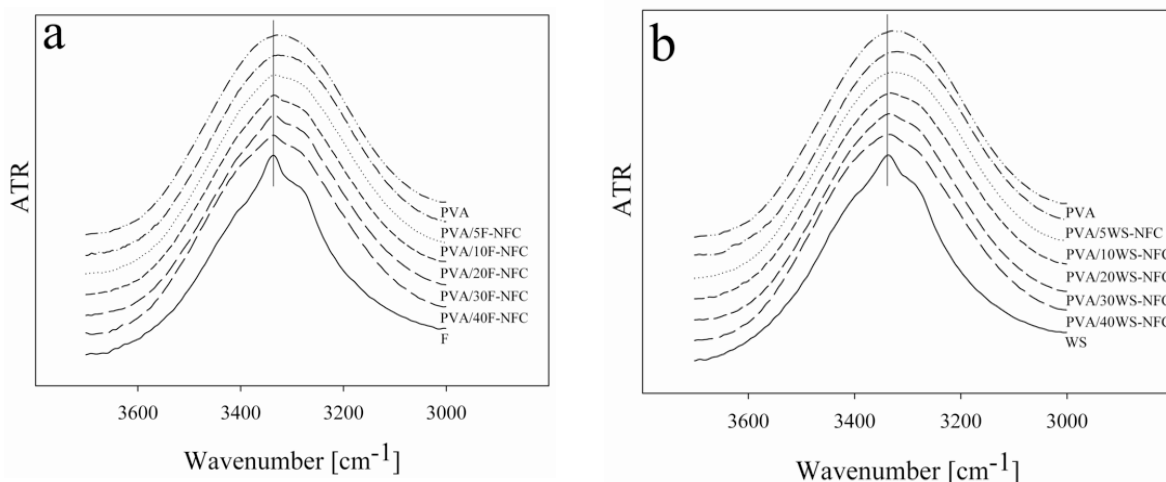


Fig. 3. Composition-dependent ATR-FTIR spectra of O-H stretching region of a) PVA, F-NFC, and PVA/F-NFC, and b) PVA, WS-NFC, and PVA/WS-NFC composites. (Absorbance scale is not given because spectra are shifted parallel.)

With increasing NFC mass fractions the O-H stretching bands became narrower and gradually shifted to higher wavenumbers, up to a wavenumber that corresponded to the cellulose O-H stretching band (3336 cm^{-1}). This peak position was reached at $w_C = 20\%$ F-NFC, and at $w_C = 30\%$ of WS-NFC, respectively. Narrowing of O-H stretching bands indicated a more regular structure of the composite with even distances of H-bonds or a reduction of interactions between PVA and NFC. This was probably covered by interactions within the neat materials, combined with a decline in PVA crystallinity. With increasing NFC content in the PVA matrix the shoulder assigned to O(6)-H(6)···O(3) intermolecular H-bonding in the cellulose NFC (3270 cm^{-1}) (Fengel 1993) became more evident.

Morphology of the composites

Scanning electron microscopy of cryo-fractured surfaces of PVA/NFC composites was done to characterize cellulose dispersion in the PVA matrix (Fig. 4). No voids signifying cellulose pull-outs were observed for composites with a cellulose content up to $w_C = 20\%$ (Fig. 4 a-d). The fracture surfaces appeared smooth. This was not observed for composites having higher cellulose contents (Fig. 4 e, f). It is also seen from the NFC fibre pullouts in PVA matrix that WS-NFC fibres were bigger than F-NFC fibres. The latter were homogeneously dispersed in the PVA matrix. WS-NFC in PVA matrix tended to agglomerate within the entire mass fraction range and its dispersion was poorer. The

arrow in Fig. 4 d marks the region of WS-NFC aggregation/sedimentation in the PVA matrix. Dispersion of cellulose in aqueous suspension should improve along with the degree of cellulose refinement (Seydibeyoğlu and Oksman 2008). Therefore, the poorer dispersion of WS-NFC in PVA compared to PVA/F-NFC composite is most likely related to a coarser structure of WS-NFC.

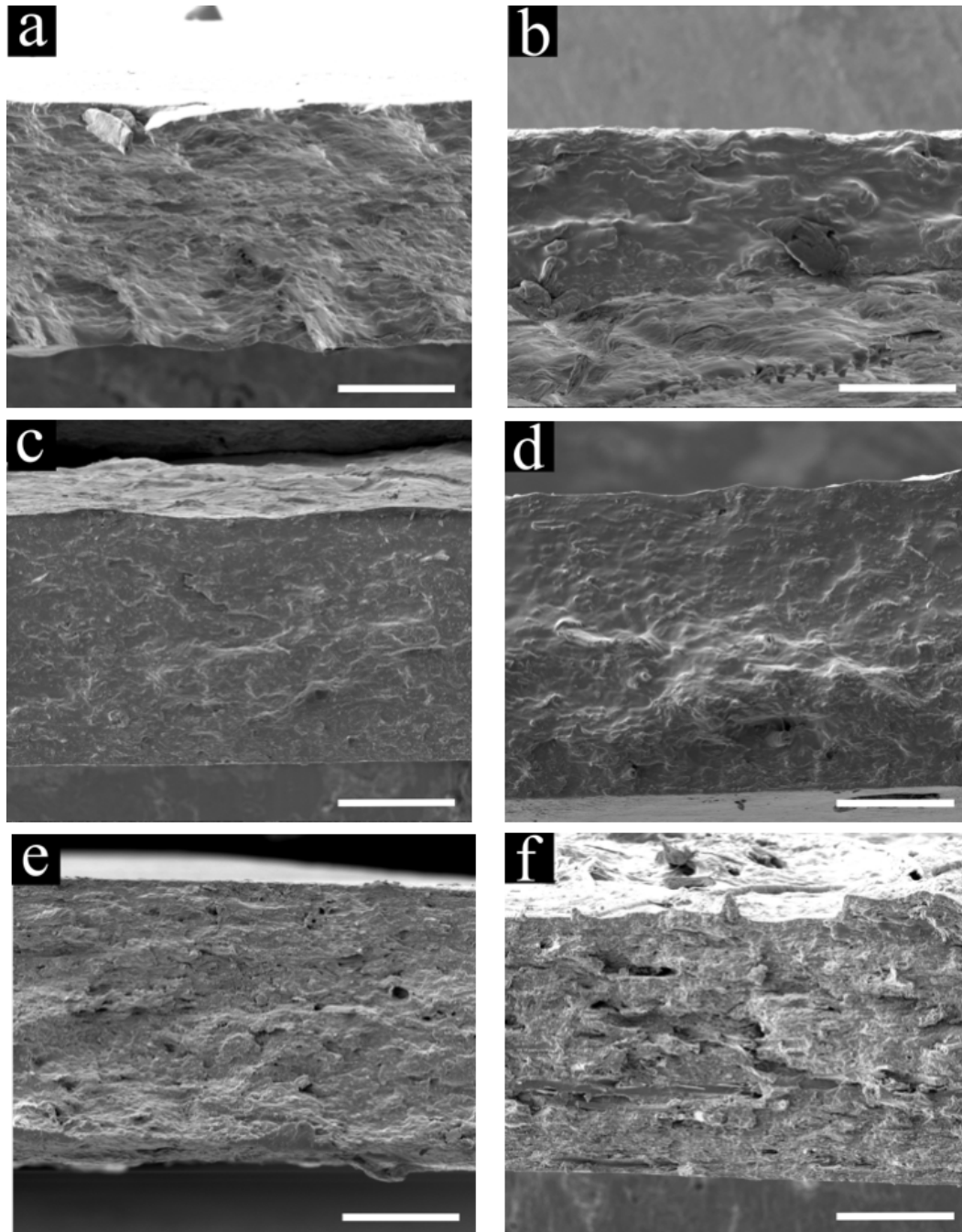


Fig. 4. SEM micrographs of cryogenic fracture surfaces PVA/NFC films a) PVA/10F-NFC, b) PVA/10WS-NFC, c) PVA/20F-NFC, d) PVA/20WS-NFC, e) PVA/40F-NFC, f) PVA/40WS-NFC. The white scale bar represents the length of 50 μm

Table 5. Results of Relative Water Uptake at Equilibrium and the Time Needed to Reach Equilibrium Swelling

Sample	Time [h]	wt. %	Sample	Time [h]	wt. %
PVA	48	5.2	PVA	48	5.2
PVA/5F-NFC	6	7.4	PVA/5WS-NFC	6	7.1
PVA/10F-NFC	48	6.2	PVA/10WS-NFC	48	6.3
PVA/20F-NFC	48	5.8	PVA/20WS-NFC	48	5.7
PVA/30F-NFC	48	5.4	PVA/30WS-NFC	48	5.4
PVA/40F-NFC	48	4.9	PVA/40WS-NFC	48	5.1
F-NFC	30	3.6	WS-NFC	30	4.3

Water sensitivity

Table 5 gives the results for relative water uptake at 50% relative humidity and 23°C, with the time needed to reach equilibrium. Water uptake was performed to observe the water sensitivity of the films at moderate humidity (50%).

Data revealed that PVA films were more sensitive to moisture than NFC films, with no marked differences between F-NFC and WS-NFC. PVA/NFC films having 5% NFC mass fraction were most sensitive to moisture, and equilibrium moisture content was reached already after 6 hours of exposure. For both NFC types the relative water uptake tended to decline as the NFC mass fraction went up. The decrease of water uptake might be linked to the formation of a continuous cellulosic structure in PVA matrix and thus a less disturbed and less moisture accessible PVA structure by contrast to the films with 5% NFC mass fraction. Similar results were reported for starch/tunicin whiskers nanocomposites. With an increasing content of whiskers in starch matrix the water uptake at equilibrium decreased, which was linked to a higher formation of a microfibrillar network (Anglès and Dufresne 2000). The formation of cellulose continuous structure was also proposed on the basis of ATR-FTIR measurements by observing the OH stretching region. The effect of different RH on properties of PVA/nanocellulose composites was described elsewhere (Roohani et al. 2008).

Thermal properties of the composites

DSC measurements were accomplished for the PVA and PVA/NFC films. Figure 5 shows that changes in melting temperatures (T_m) of the composite films as well as heat of fusion (ΔH_m) were similar across the different compositions, irrespective of the used NFC reinforcement. Heat of fusion was calculated with respect to the PVA content in the composite. For composites having $w_C = 5\%$ and 10% , respectively, ΔH_m increased compared to the neat PVA. This can be ascribed to the nucleating ability of the fibrils (Lu et al. 2008). With higher amounts of NFCs ΔH_m of PVA matrix unambiguously declined. As can be seen in Figure 5, the melting temperature varied only slightly. T_m reflects the nature of the crystalline structure. Lowering of T_m is a consequence of restricted spherulite growth or crystalline imperfection. However, in some composite systems, especially in good miscible systems, the decrease of melting temperature confirms specific interactions between the blended components (Dubief et al. 1999; Nishio et al.

1989; Roohani et al. 2008; Samir et al. 2004). T_m decreased despite the increasing ΔH_m . Therefore, due to the similar nature of filler and matrix, it is reasonable to ascribe the drop of T_m to interactions between composite components. This result agreed well with the interaction revealed by ATR-FTIR.

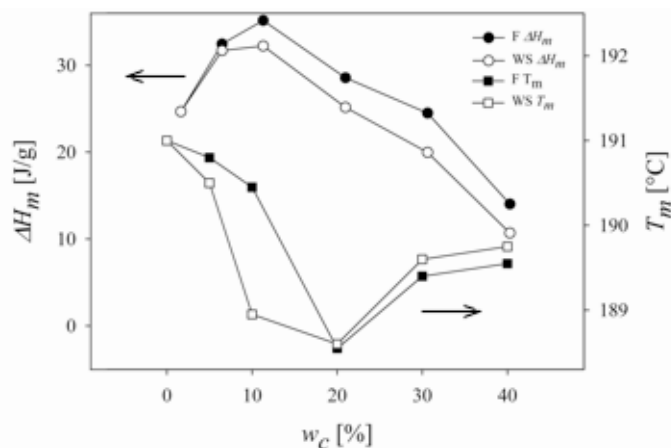


Fig. 5. Melting temperatures (T_m) and heat of fusion (ΔH_m) of the PVA matrix in relation to the cellulose mass fraction

Viscoelastic properties of the composites

The study of viscoelastic properties was focused on the relaxation range close to the glass transition of PVA. As shown in Fig. 6, the concentration-dependant effect of NFC type on viscoelastic properties of PVA/NFC composites is obvious in every single region of viscoelastic behaviour. Table 5 provides numerical results for dynamic-mechanical analyses, i.e. storage modulus at 20 °C and 100 °C, respectively. The table also lists T_g as well as $\tan \delta$ height for both PVA and PVA/NFC films. In the glassy region even the presence of 5% mass fraction of NFC resulted in remarkably higher mechanical properties of the composite, compared to neat matrix. E' at 20 °C was 1.7 and 1.8 times higher for the F-NFC and WS-NFC reinforced PVA composites, respectively, compared to the PVA reference (Table 6). Upward drift of the E' in the glassy region with increasing mass fraction of NFC was observed for both materials. With a reinforcement between $w_C = 30\%$ and 40% the WS-NFC reinforcement was distinctly stronger than F-NFC, and reached almost a threefold improvement over neat PVA. Higher E' in the glassy region might be a consequence of higher DP of WS-NFC, which is a known factor for cellulose stiffness.

The stiffness increase in the rubbery region (E' at 100 °C) was distinct for both materials and reached more than a thirtyfold increase with $w_C = 10\%$, exceeding the initial value of PVA by over a factor of 100 with $w_C = 40\%$. The mechanical restraint in the rubbery region was more pronounced for the PVA/F-NFC compared to PVA/WS-NFC. Such behaviour was described by others and the improvement of mechanical performance as well as the thermal stability was attributed either to the percolation effect, or to a tangling effect of cellulose microfibrils (Dubief et al. 1999; Samir et al. 2004). Another explanation is the existence of intermolecular interactions between cellulose and the polymer matrix (Shibayama et al. 1991). However, better performance of PVA/F-

NFC composites in the rubbery region is most likely based on better dispersion of the F-NFC in the PVA matrix, as demonstrated through SEM (cp. Fig. 4).

Table 6. DMA Results: Storage Modulus in Glassy and Rubbery Regions, Glass Transition and Height of Loss Tangent Peak of PVA, PVA/F-NFC, and PVA/WS-NFC Composites

Sample	E' at 20 °C [GPa]	E' at 100 °C [GPa]	T_g [°C]	$\tan \delta$ (height)
PVA	2.42	0.01	50.5	0.456
PVA/5F-NFC	4.12	0.21	51.7	0.335
PVA/10F-NFC	4.39	0.46	56.4	0.291
PVA/20F-NFC	5.84	0.90	58.8	0.205
PVA/30F-NFC	5.42	1.12	60.7	0.203
PVA/40F-NFC	6.18	1.92	60.9	
PVA/5WS-NFC	4.41	0.17	53.9	0.359
PVA/10WS-NFC	4.81	0.39	53.8	0.261
PVA/20WS-NFC	5.59	0.59	58.4	0.296
PVA/30WS-NFC	6.66	0.80	58.4	0.193
PVA/40WS-NFC	7.16	1.51	58.3	0.187

As shown in Fig. 6 the relaxation region was broadened with shifts to higher temperatures as NFC mass fraction increased. The effect of crystallinity on E' was blocked due to decreasing PVA crystallinity with NFC content. T_g of PVA/WS-NFC composites leveled off at 58 °C and $w_C = 20\%$; and T_g of PVA/F-NFC composite equalized at $w_C = 30\%$, reaching almost 61 °C, which was 10 °C above that of neat PVA. The strong decrease of the $\tan \delta$ peak as a consequence of cellulose insertion into the PVA matrix is an indicator of good adhesion between filler and matrix (Gregorova et al. 2010; Hrabalova et al. 2010; Keusch and Haessler 1999; Pothan et al. 2003). Interestingly, the height of the $\tan \delta$ peak was similar irrespective to the used NFC type. This result might lead to the conclusion that hydrogen bonding formed within the composite is a decisive factor impacting $\tan \delta$. The effect of hydrogen bonding on $\tan \delta$ was reported earlier by, e.g., Huda et al. (2008).

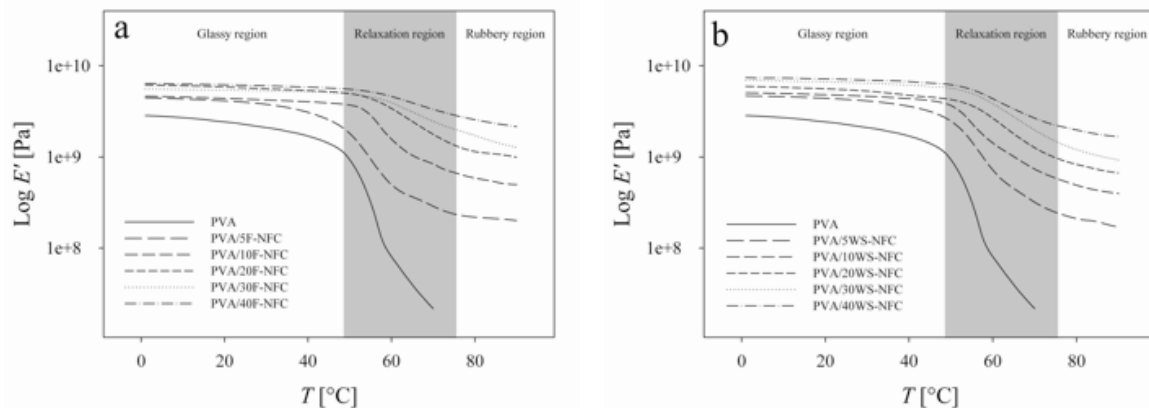


Fig. 6. Logarithm of the storage modulus E' versus temperature at 1Hz for a) PVA/F-NFC and b) PVA/WS-NFC at NFC mass fractions in the range between 5 and 40%

CONCLUSIONS

Disintegration of flax and wheat straw cellulose pulps by a high pressure homogenizer was investigated. Materials were prepared in order to evaluate the effect of nanofibrillated celluloses (NFCs) on the properties of their polyvinyl alcohol (PVA) composites. The suitability of flax cellulose pulp and wheat straw cellulose pulp for high pressure disintegration was investigated, as well as the reinforcing potential of disintegrated NFCs.

1. It was shown that the production of NFC from wheat straw (WS-NFC) might be inferior to that obtained from flax without additional pre-treatment of the raw material (e.g. chemical). Such production is technically demanding, tedious, and time-consuming. The less demanding disintegration of flax cellulose was most probably due to the lower DP of its cellulose component.
2. The PVA/WS-NFC showed a better storage modulus in glassy region only. The better mechanical performance of the flax-containing PVA/F-NFC composites in rubbery region was most probably related to better dispersion of F-NFC in the PVA matrix. T_g , determined from DMA, was improved due to the presence of NFC. T_g increased with w_c for both materials.
3. As concluded from SEM micrographs, the more homogeneous dispersion in PVA was better reached with F-NFC, as compared to the WS-NFC dispersion. The better dispersion of F-NFC is explained by its higher fineness.
4. Water sensitivity measurements showed that at 50% RH and 23°C the most sensitive composites were those having 5% NFC. Water sensitivity declined at higher NFC mass fractions.
5. Inter-polymer bonding between NFCs and PVA hydroxyl groups was supported by DSC and ATR-FTIR. Both methods showed inter-polymer bonding as most pronounced up to $w_c = 20\%$ NFC. It is suggested that at higher NFC contents ($w_c > 20\%$) interactions within each component apart are more pronounced than inter-polymer interactions between PVA and NFCs.

ACKNOWLEDGEMENTS

This work was financed by Austrian Science Fund (FWF, Project L319-B16) and COST Action E50 CEMARE (ref. no. COST-STSM-E50-4325). Thanks are due to Esther Strub from the Wood Laboratory at EMPA, Dübendorf, Switzerland, for her help with viscosity measurements and FE-SEM.

REFERENCES CITED

- Anglès, M. N., and Dufresne, A. (2000). "Plasticized starch/tunicin whickers nanocomposites. 1. Structural analysis," *Macromolecules* 22(33), 8344-8353.

- Anonymous (2004). "Pulps – Determination of limiting viscosity number in cupriethylenediamine (CED) solution," In ISO. *ISO 5351*: ISO.
- Bruce, D. M., Hobson, R. N., Farrent, J. W., and Hepworth, D. G. (2005). "High-performance composites from low-cost plant primary cell walls," *Composites Part A: Applied Science and Manufacturing* 36(11), 1486-1493.
- Charlet, K., Jernot, J. P., Eve, S., Gomina, M., and Bréard, J. (2010). "Multi-scale morphological characterisation of flax: From the stem to the fibrils," *Carbohydrate Polymers* 82(1), 54-61.
- Dubief, D., Samain, E., and Dufresne, A. (1999). "Polysaccharide microcrystals reinforced amorphous poly(beta-hydroxyoctanoate) nanocomposite materials," *Macromolecules* 32(18), 5765-5771.
- Erukhimovitch, V., Talyshinsky, M., Souprun, Y., and Huleihel, M. (2006). "FTIR spectroscopy examination of leukemia patients plasma," *Vibrational Spectroscopy* 40, 40-46.
- Favier, V., Chanzy, H., and Cavaille, J. Y. (1995). "Polymer nanocomposites reinforced by cellulose whiskers," *Macromolecules* 28(18), 6365-6367.
- Fengel, D. (1993). "Influence of water on the OH valency range in deconvoluted FTIR spectra of cellulose," *Holzforschung* 47, 103-108.
- Galya, T., Sedlařík, V., Kuřitka, I., Novotný, R., Sedlaříková, T., and Sába, P. (2008). "Antibacterial poly(vinyl alcohol) film containing silver nanoparticles: Preparation and characterization," *Journal of Applied Polymer Science* 110(5), 3178-3185.
- Gregorova, A., Hrabalova, M., Kovalcik, R., and Wimmer, R. (2011). "Surface modification of spruce wood flour and effects on the dynamic fragility of PLA/wood composites," *Polymer Engineering & Science* 51, 143-150.
- Helbert, W., Cavaille, J. Y., and Dufresne, A. (1996). "Thermoplastic nanocomposites filled with wheat straw cellulose whiskers. 1. Processing and mechanical behavior," *Polymer Composites* 17(4), 604-611.
- Henriksson, M. (2008). "Cellulose nanofibril networks and composites. Preparation, structure and properties," *KTH Chemical Science and Engineering* (p. 61).
- Hrabalova, M., Gregorova, A., Wimmer, R., Sedlarik, V., Machovsky, M., and Mundigler, N. (2010). "Effect of wood flour loading and thermal annealing on viscoelastic properties of poly(lactic acid) composite film," *Journal of Applied Polymer Science, in press* (DOI: 10.1002/app.32509).
- Huda, M. S., Drzal, L. T., Mohanty, A. K., and Misra, M. (2008). "Effect of fiber surface treatments on the properties of laminated biocomposites from poly(lactic acid) (PLA) and kenaf fibers," *Compos Sci. Tech.* 68, 424.
- Iwamoto, S., Nakagaito, A. N., and Yano, H. (2007). "Nano-fibrillation of pulp fibers for the processing of transparent nanocomposites," *Applied Physics A: Materials Science & Processing* 89(2), 461-466.
- Keusch, S., and Haessler, R. (1999). "Influence of surface treatment of glass fibres on the dynamic mechanical properties of epoxy resin composites. *Composites Part A: Applied Science and Manufacturing* 30(8), 997-1002.
- Klemm, D., Schumann, D., Kramer, F., Hessler, N., Koth, D., and Sultanova, B. (2009). "Nanocellulose materials – Different cellulose, different functionality," *Macromol. Symp.* 280, 60-71.

- Kondo, T., Sawatari, C., Manley, R. S., and Gray, D. G. (1994). "Characterization of hydrogen-bonding in cellulose synthetic-polymer blend systems with regioselectively substituted methylcellulose," *Macromolecules* 27(1), 210-215.
- Leitner, J., Hinterstoisser, B., Wastyn, M., Keckes, J., Gindl, W. (2007). "Sugar beet cellulose nanofibril-reinforced composites," *Cellulose* 14(5), 419-425.
- Liu, R. G., Yu, H., and Huang, Y. (2005). "Structure and morphology of cellulose in wheat straw," *Cellulose* 12(1), 25-34.
- Lu, J., Wang, T., and Drzal, L. T. (2008). "Preparation and properties of microfibrillated cellulose polyvinyl alcohol composite materials," *Composites Part A: Applied Science and Manufacturing* 39(5), 738-746.
- Maréchal, Y., and Chanzy, H. (2000). "The hydrogen bond network in I_β cellulose as observed by infrared spectrometry," *Journal of Molecular Structure* 523, 183-196.
- Marx-Figini, M. (1978). "Significance of the intrinsic viscosity ratio of unsubstituted and nitrated cellulose in different solvents," *Die Angewandte Makromolekulare Chemie*, 72, 161-171.
- Millon, L. E., and Wan, W. K. (2006). "The polyvinyl alcohol-bacterial cellulose system as a new nanocomposite for biomedical applications," *Journal of Biomedical Materials Research Part B-Applied Biomaterials* 79B(2), 245-253.
- Moore, G. F., and Saunders, S. M. (1997). *Advances in Biodegradable Polymers*. Rapra Publishing.
- Nakagaito, A. N., and Yano, H. (2004). "The effect of morphological changes from pulp fiber towards nano-scale fibrillated cellulose on the mechanical properties of high-strength plant fiber based composites," *Applied Physics A: Materials Science & Processing* 78(4), 547-552.
- Nakagaito, A. N., and Yano, H. (2005). "Novel high-strength biocomposites based on microfibrillated cellulose having nano-order-unit web-like network structure," *Applied Physics A* 80, 155-159.
- Nishio, Y., Hirose, N., and Takahashi, T. (1989). "Thermal-analysis of cellulose poly(ethylene oxide) blends," *Polymer Journal* 21(4), 347-351.
- Pothan, L. A., Oommen, Z., and Thomas, S. (2003). "Dynamic mechanical analysis of banana fiber reinforced polyester composites," *Composites Science and Technology* 63(2), 283-293.
- Roohani, M., Habibi, Y., Belgacem, N. M., Ebrahim, G., Karimi, A. N., and Dufresne, A. (2008). "Cellulose whiskers reinforced polyvinyl alcohol copolymers nanocomposites," *European Polymer Journal* 44(8), 2489-2498.
- Rowell, R. M., Han, J. S., and Rowell, J. S. (2000). "Characterisation and factors effecting fiber properties," *Natural Polymers and Agrofibers Based Composites*, 115-134.
- Samir, M. A. S. A., Alloin, F., and Dufresne, A. (2005). "Review of recent research into cellulosic whiskers, their properties and their application in nanocomposite field," *Biomacromolecules* 6(2), 612-626.
- Samir, M. A. S. A., Alloin, F., Paillet, M., and Dufresne, A. (2004). "Tangling effect in fibrillated cellulose reinforced nanocomposites," *Macromolecules* 37(11), 4313-4316.

- Sawatari, C., and Kondo, T. (1999). "Interchain hydrogen bonds in blend films of poly(vinyl alcohol) and its derivatives with poly(ethylene oxide)," *Macromolecules*, 32(6), 1949-1955.
- Schartel, B., Wendling, J., and Wendorff, J. H. (1996). "Cellulose poly(vinyl alcohol) blends. 1. Influence of miscibility and water content on relaxations," *Macromolecules* 29(5), 1521-1527.
- Schultz, T. P., McGinnis, G. D., and Bertran, M. S. (1985). "Estimation of cellulose crystallinity using Fourier transform infrared spectroscopy and dynamic thermogravimetry," *Journal of Wood Chemistry and Technology* 5(4), 543-557.
- Schwanninger, M., Rodrigues, J., Pereira, H., and Hinterstoisser, B. (2004). "Effects of short-time vibratory ball milling on the shape of FT-IR spectra of wood and cellulose," *Vibrational Spectroscopy* 36(1), 23-40.
- Seydibeyoğlu, M. Ö., and Oksman, K. (2008). "Novel nanocomposites based on polyurethane and micro fibrillated cellulose," *Composites Science and Technology*, 68(3-4), 908-914.
- Shibayama, M., Yamamoto, T., Xiao, C. F., Sakurai, S., Hayami, A., and Nomura, S. (1991). "Bulk and surface characterization of cellulose poly(vinyl alcohol) blends by Fourier-transform infrared-spectroscopy," *Polymer* 32(6), 1010-1016.
- Siró, I., and Plackett, D. (2010). "Microfibrillated cellulose and new nanocomposite materials: A review," *Cellulose* 17(3), 459-494.
- Tadoroko, H. (1959). "Infrared studies of polyvinyl alcohol by deuteration of its OH groups," *Bulletin of the Chemical Society of Japa*, 32(11), 1252-1257.
- Tímár-Balázsy, A., and Eastop, D. (2002). *Chemical Principles of Textile Conservation*. Butterworth-Heinemann.
- Yu, L., Dean, K., and Li, L. (2006). "Polymer blends and composites from renewable resources," *Progress in Polymer Science* 31(6), 576-602.
- Zhu, B., Li, J. C., He, Y., and Inoue, Y. (2003). "Studies on binary blends of poly (3-hydroxybutyrate-co-3-hydroxyhexanoate) and natural polyphenol catechin: Specific interactions and thermal properties," *Macromolecular Bioscience* 3(5), 258-267.
- Zimmermann, T., Bordeanu, N., and Strub, E. (2010). "Properties of nanofibrillated cellulose from different raw materials and its reinforcement potential," *Carbohydrate Polymers* 79(4), 1086-1093.
- Zimmermann, T., Pöhler, E., and Geiger, T. (2004). "Cellulose fibrils for polymer reinforcement," *Advanced Engineering Materials* 6(9), 754-761.

Article submitted: November 27, 2010; Peer review completed: February 24, 2011;
Revised version received and accepted: March 22, 2011; Published: March 23, 2011.